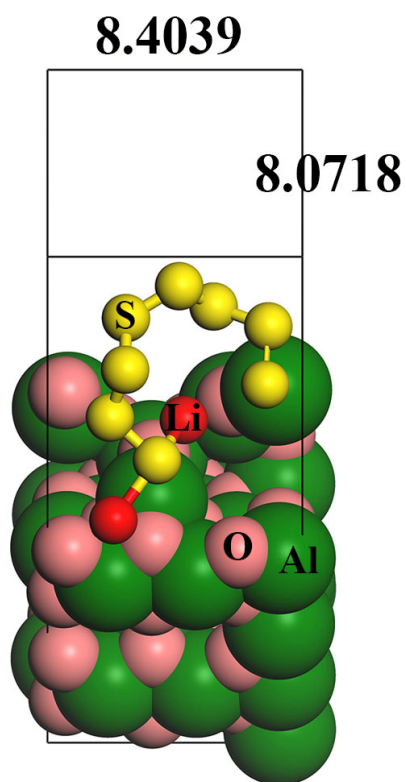
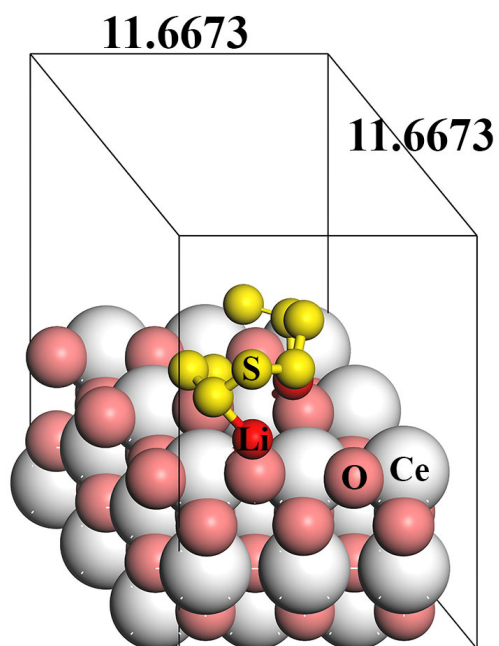


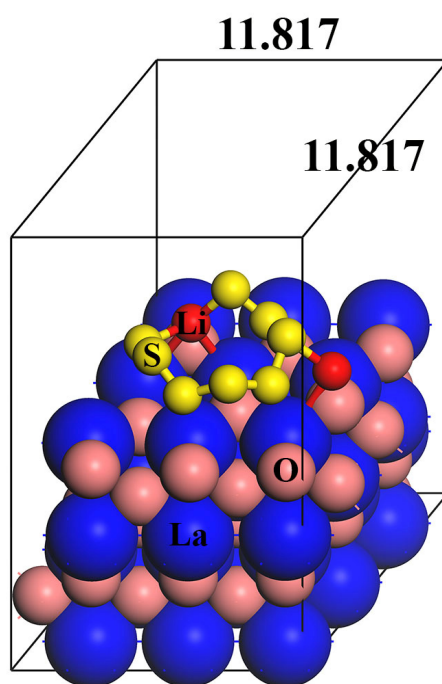
**Supplementary Figure 1 | SEM image of the cycled composite electrodes based on Al<sub>2</sub>O<sub>3</sub>/C.** Abundant Li<sub>2</sub>S particles with irregular shape were formed between the Al<sub>2</sub>O<sub>3</sub>/C nanoflakes after 100 cycles. Only few Li<sub>2</sub>S film can be deposited on the surface of Al<sub>2</sub>O<sub>3</sub>/C, indicating the uncontrolled deposition of Li<sub>2</sub>S.



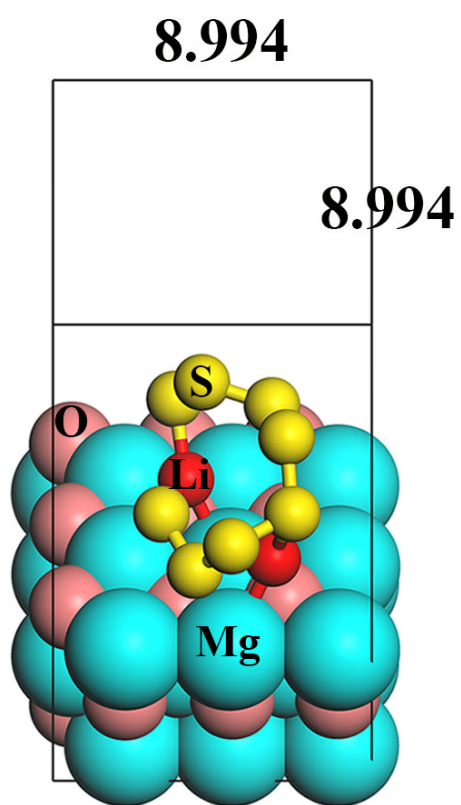
Supplementary Figure 2 | Optimized geometries of most stable  $\text{Li}_2\text{S}_8$  on  $\text{Al}_2\text{O}_3(110)$ .



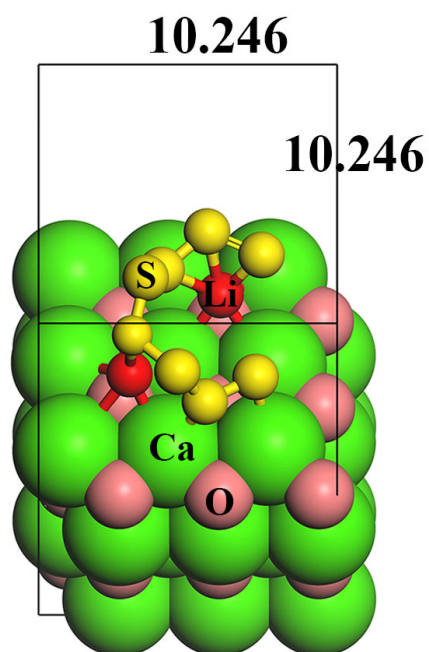
Supplementary Figure 3 | Optimized geometries of most stable  $\text{Li}_2\text{S}_8$  on  $\text{CeO}_2(111)$ .



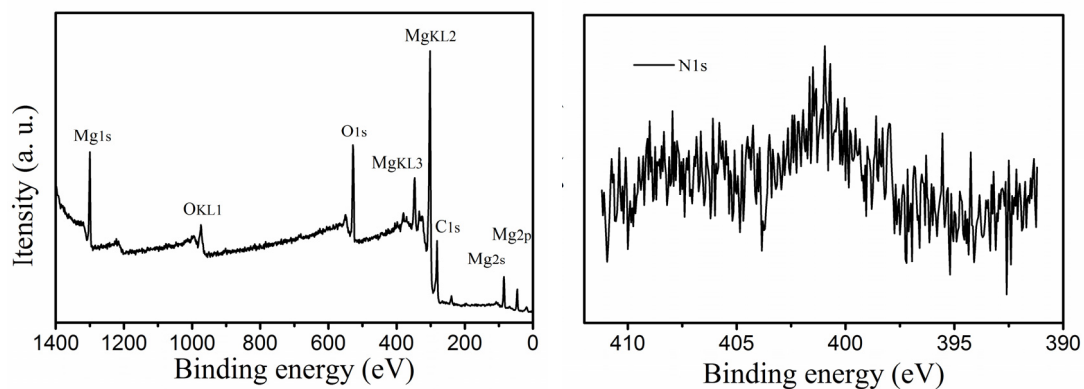
Supplementary Figure 4 | Optimized geometries of most stable Li<sub>2</sub>S<sub>8</sub> on La<sub>2</sub>O<sub>3</sub>(001).



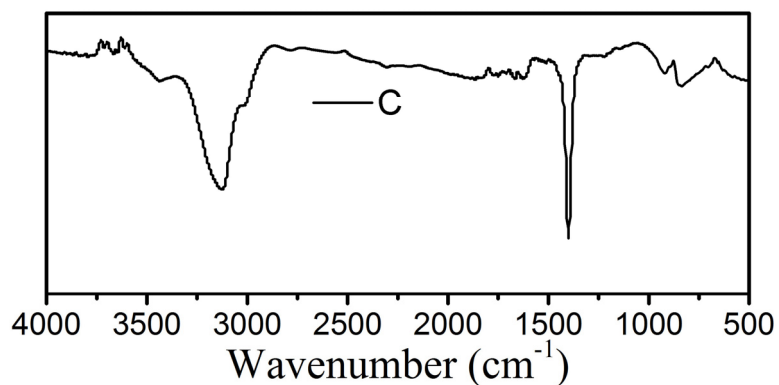
Supplementary Figure 5 | Optimized geometries of most stable  $\text{Li}_2\text{S}_8$  on  $\text{MgO}(100)$ .



Supplementary Figure 6 | Optimized geometries of most stable Li<sub>2</sub>S<sub>8</sub> on CaO(100).

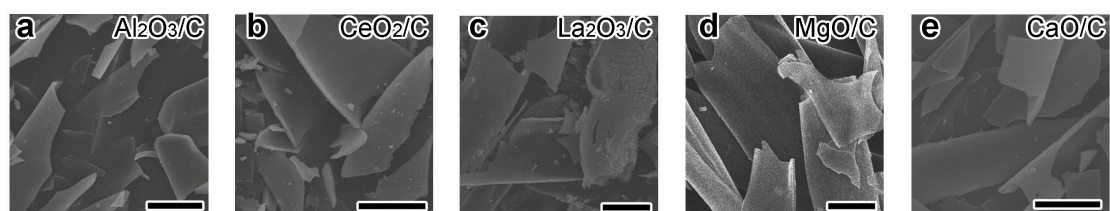


**Supplementary Figure 7 | XPS characterization of MgO/C sample.** Representative survey scan XPS spectrum of the MgO/C (left), indicating that the sample contains mainly Mg, O and C. No obvious N signal can be detected in the survey spectrum. The high resolution XPS spectrum for N1s of the MgO/C sample (right) reveals that trace oxygen (<0.7 wt%) can be detected. Similar phenomena were found for the other oxide/carbon samples.



**Supplementary Figure 8 | Representative FTIR spectra of pure C sample derived from Kapok fibers.** The peaks at 3123 and 1380  $\text{cm}^{-1}$  can be ascribed to the existence of  $-\text{OH}$ . Similar peaks can be observed in all oxide/carbon composite samples. Because Kapok fibers are chemically composed of 64% cellulose ( $(\text{C}_6\text{H}_{10}\text{O}_5)_n$ ), 13% lignin, and 23% pentosan. Residual  $-\text{OH}$  will be remained during the pyrolysis of fibers. This kind of surface group will be beneficial to the strong bonding between the metal oxide nanoparticles and carbon matrix.





**Supplementary Figure 9 | Representative SEM images of the composites after grinding.** Abundant carbon flakes can be obtained after the grinding of the composite fibers (scale bar, 10  $\mu\text{m}$ ). No obvious difference can be found for these oxide/carbon composites. Compared with the sulfur/oxide/carbon composite (Fig. 5), the flakes in supplementary Fig. 9 have bigger size. This is because that the sulfur loaded oxide/carbon composite has been grinded again to prepare the slurry for the cathode.

**Supplementary Table 1 | Li<sub>2</sub>S<sub>8</sub> capture results of metal oxide nanoparticles.** Adsorption percentage of Li<sub>2</sub>S<sub>8</sub> (0.005M, 2 ml) by different metal oxide nanoparticles with the same total surface area (1.6 m<sup>2</sup>) at different temperatures based on the ICP-OES test.

	Al <sub>2</sub> O <sub>3</sub>	CeO <sub>2</sub>	La <sub>2</sub> O <sub>3</sub>	MgO	CaO
Adsorption percentage at 35 °C	77.6 %	75.5 %	65.8 %	67.9 %	44.5 %
Adsorption percentage at 60 °C	79.1 %	76.9 %	66.5 %	68.5 %	45.0 %

**Supplementary Table 2 | Li<sub>2</sub>S<sub>8</sub> capture results of carbon nanocomposites.** Adsorption percentage of Li<sub>2</sub>S<sub>8</sub> by different metal oxide/carbon nanocomposites with the same mass (0.015g) based on the ICP-OES test.

	Al <sub>2</sub> O <sub>3</sub> /C	CeO <sub>2</sub> /C	La <sub>2</sub> O <sub>3</sub> /C	MgO/C	CaO/C	C
Adsorption percentage	83.5 %	80.1 %	64.7 %	81.2 %	55.3 %	11.1%